Subtle effects control the polymerisation mechanism in α-diimine iron catalysts

Mikael P. Johansson [a,b,*] *and Marcel Swart* [a,c,*]

[a] Institut de Química Computacional and Departament de Química, Universitat de Girona, Campus Montilivi, ES-17071 Girona, Spain

[b] Laboratory for Instruction in Swedish, Department of Chemistry, University of Helsinki, FI-00014 Helsinki, Finland

[c] Institució Catalana de Recerca i Estudis Avançats (ICREA), Barcelona, Spain

e-mail: mikael.johansson@iki.fi, marcel.swart@icrea.cat

31 May 2011

TITLE RUNNING HEAD: Subtle effects in α-diimine iron catalysts

ABSTRACT α-diimine iron complexes have been suggested to catalyse polymerisation *via* two distinct pathways, depending on the spin state of the iron complex. Here, we study a typical complex of this family, $^{R"}$[*N*,*N*]$FeCl_2$, with [*N*,*N*] = Cy–N=CR"–CR"=N–Cy (Cy=cyclohexyl, R"=PhF (*para*-fluorophenyl), PhOMe (*para*-methoxyphenyl), $PhNMe_2$ (*para*-dimethylaminophenyl). With R"=PhF, PhOMe, polymerisation proceeds as a catalytic chain transfer (CCT) mechanism, with R"=$PhNMe_2$, the polymerisation follows an atom transfer radical polymerisation (ATRP) pathway. Contrary to previous suggestions, we show that the spin-states of the complexes involved are not affected by the R" group. Instead, the different behaviour arises from a subtle interplay between the electron-withdrawing or donating character of the reasonably distant phenyl substituent and the iron centre, and small but crucial differences in the reorganisation energies effected during the reactions.

1. Introduction

Recently, Gibson and co-workers extended the applicability of metal spin-state controlled catalysis beyond the realm of biomolecules, by showing that very different catalytic behaviour can be expressed also in non-biological, industrial applications.[1] In subsequent work, the catalytic details of this family of α-diimine iron complexes, with the general formula $^{R',R"}$[*N*,*N*]$FeCl_2$ ($^{R',R"}$[*N*,*N*] = R'–N=CR"–CR"=N–R'), with various R' and R" groups has been elucidated.[2-4] In these catalysts, two different polymerisation pathways have been observed. One proceeds mainly as an atom transfer radical polymerisation (ATRP),[5-7] and the other follows a catalytic chain transfer (CCT)[8-10] mechanism. One mechanism is favoured over the other, depending on the R' and R" ligands. Electron-withdrawing R" groups favour CCT, and electron-donating groups favour ATRP. It was suggested that the spin-state of the iron, formally in oxidation state III in the intermediate complexes, would be the deciding factor governing the reaction. This spin-state was different depending on the character of the varying ligands; the CCT reactions go through a rare intermediate-spin (S=3/2) complex, and the ATRP reactions have a more common high-spin (S=5/2) intermediate.[1-4]

To assess this intriguing interplay between the relatively distant phenyl substituent and the catalytic centre around iron, seven bonds and more than eight Ångströms away, a quantum chemical investigation of the systems can potentially reveal details not accessible by experiment. Modelling these reactions presents a challenge, however. For a reliable description of the energetics and properties, a full quantum approach is necessary. Further, thermal corrections need to be considered. This is important not only for finite temperature reaction energetics, but also to explore the possibility of spin-transitions, *i.e.*, crossover to higher spin states with increasing temperature.[11-14] From a computational point of view, the systems are problematic in three ways: *(i)* the molecules are reasonably large, *(ii)* they contain a transition metal, and *(iii)* the energy difference between spin states is a crucial property. The system size rules out the use of very high-level *ab initio* wave-function methods, like coupled-cluster theory, even for the electronic ground state at 0 K, not to mention geometry optimisation and the calculation of the vibrational spectrum, necessary for thermal corrections. In practice, three methods remain: Hartree–Fock (HF),[15,16] second-order Møller–Plesset perturbation theory (MP2),[17,18] and density functional theory (DFT).[19,20] The transition metal present, and the need for a proper description of spin states and radicals rule out the HF method, which neglects the effects of electron correlation. The correlated MP2 method, while often successful for organic reactions, is also not applicable due to poor performance when transition metals are involved. This leaves DFT. Until recently, the requirement of reliable spin-state energetics would have prevented, or at least cast doubt on the applicability also of this approach. Progress in the field of DFT is, however, still rapid, and new functionals with improved capabilities become available. In this context, the new Swart–Solà–Bickelhaupt (SSB-D)[21] functional is of special interest, as it has been shown to provide very reliable relative spin-state energies for various iron complexes.[21,22] Further, the functional exhibits robust performance for reaction barriers[23] and hydrogen bonding, and by incorporating the dispersion correction by Grimme,[24] weak interactions are described satisfactorily.[25] The good performance for magnetisabilities[26] and nuclear magnetic resonance[27] underlines the general-purpose character of SSB-D. The Becke–Perdew (BP86)[28,29] functional, on the other hand, is known to perform well for geometries[30] and vibrational frequencies[31]

of iron-complexes. BP86 also gives good spin distributions,[32-34] even if it energetically artificially favours lower spin states like most non-hybrid generalised gradient approximations.[35-40]

Here, combining the strengths of the SSB-D and BP86 functionals, we study the differences in catalytic behaviour of three representative complexes of the α-diimine iron family, $^{R',R''}$[*N*,*N*]$FeCl_2$. We use cyclohexyl as the R' ligand throughout. For the R" group, we use *para*-phenyl substituents of different character. The electron-withdrawing *para*-fluorophenyl (PhF) and the electron-donating *para*-dimethylaminophenyl ($PhNMe_2$) were, in Ref. 3, found to represent opposite extremes, PhF most clearly favouring CCT, and $PhNMe_2$ most clearly favouring ATRP. In addition, we examine the behaviour of *para*-methoxyphenyl (PhOMe), with a behaviour in-between that of the two extremes, but still found to use the CCT pathway. The aim is to get a detailed insight of how the change of phenyl substituent crucially affects the surrounding of the iron centre. We show that already the energetics of the first up-hill reactions of the complex with a model organic initiator ligand, separate the two pathways, shown in Scheme 1. Following Ref. 1, we use benzyl chloride (BnCl) as the initiator.

Scheme 1. Schematic of the two reactions studied. R"=PhF, PhOMe, $PhNMe_2$.

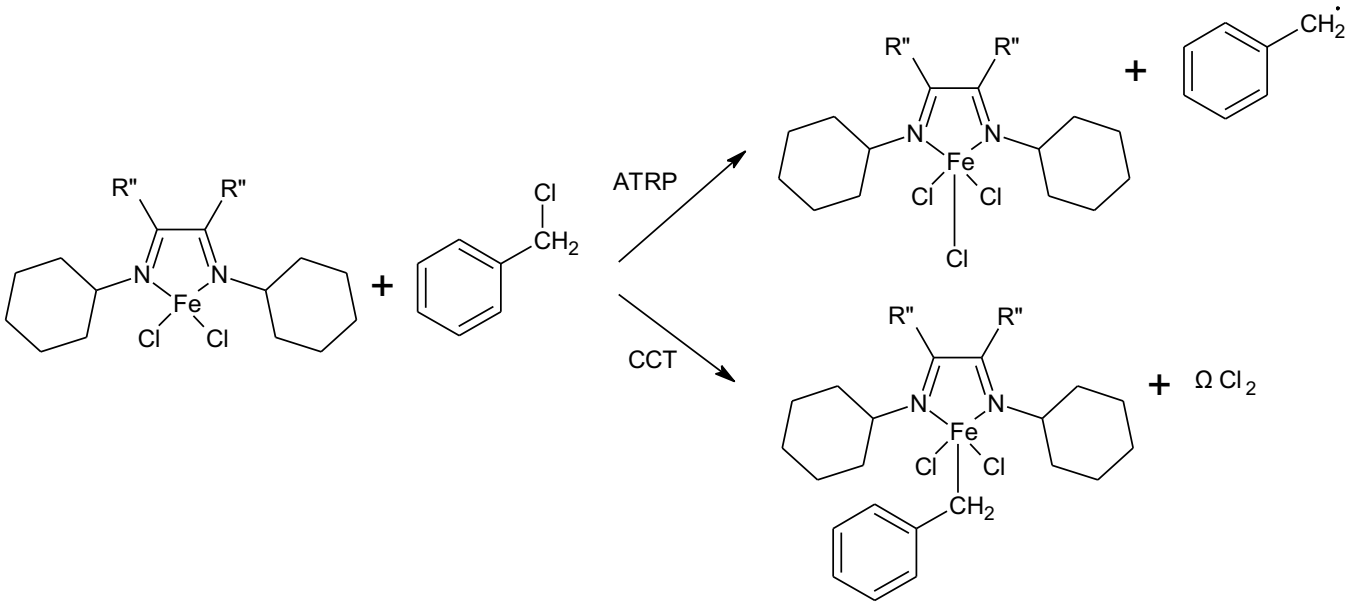

2. Computational details

All structures were optimised at density functional theory (DFT)[19,20] level, using the BP86 functional,[28,29] with the polarised triple-zeta def2-TZVP basis set,[41] employing the density-fitting resolution of the identity (RI) formalism.[42-44] The environment was accounted for by means of the COSMO electrostatic continuum model,[45] simulating a chloroform solvent (dielectric constant ε=4.8, solvent radius 3.17 Å). Final energies and electron densities were evaluated with the SSB-D functional,[21] using the polarised quadruple-zeta QZ4P basis set,[46] again using COSMO. For consistency, both the BP86 and SSB-D calculations used the dispersion correction to DFT.[24] This was recently shown to be important also for transition metal complexes.[47] Thermal corrections were computed treating rotation classically, and assuming ideal gas behaviour[48]; harmonic vibrational frequencies were computed with numerical second derivatives on separately optimised gas-phase structures. No frequency scaling was used, as this has been shown to be unnecessary for the BP86 functional.[49] The energies include the zero-point vibrational energy (ZPE), unless otherwise noted. For the reaction energies, we treat the free chlorine radical as half of a Cl_2 molecule. The produced chlorine radicals would quickly recombine, and one likely product is Cl_2. Another possibility would be hydrogen abstraction from the solvent, with the production of HCl and a solvent molecule radical. The solvent radical would, however, also be very reactive, and quickly react further.

The BP86-D calculations were performed with the TURBOMOLE package,[50,51] version 6.1 and the SSB-D calculations with the ADF package,[52,53] version 2009.01. Default convergence and threshold settings were used, with the following, tighter exceptions: The self-consistent-field (SCF) equations were converged to an energy of 10^{-7} a.u. during energy evaluations and geometry optimisations, and to 10^{-8} a.u. when computing the second derivatives; geometries were converged to a gradient norm of 10^{-4} a.u.; the BP86-D calculations used the "m4" grid,[54] and the SSB-D calculations an integration accuracy setting of 7.5.

3. Results and discussion

3.1 Molecular and electronic structure of the parent Fe(II)Cl_2 complexes

We start by considering the molecular structure of the three parent complexes, with R"=PhF, PhOMe, and $PhNMe_2$, in both the high- and intermediate-spin states. Figure 1 shows the molecular structures of selected complexes. Table 1 summarises the main structural parameters, using the naming convention for the atoms bonded to iron as depicted in Figure 1. One can see that for the same spin state, there are very little structural differences between the three complexes. The root-mean-square (RMS) deviation between the structures serves as a concise measure of the differences. For the identical backbone, that is, all atoms except those of the phenyl substituent, the RMS deviation between the superimposed structures is between 3.3 and 7.7 pm for both spin states. The geometries show a systematic change with respect to the electron affinity of the phenyl substituent, with the difference between R"=PhF, PhOMe and R"=PhOMe, $PhNMe_2$ being roughly half of the difference between R"=PhF, $PhNMe_2$.

A substantial difference occurs when the spin state changes, however. As expected, the iron in the high-spin state expands compared to the intermediate-spin state. The Fe–N bonds show the largest difference, while the Fe–Cl bond lengths are almost unaffected. Instead, the Cl–Fe–Cl angle increases substantially. One can also note a large difference in the position of the iron relative to the N-C=C-N plane. In the high-spin state, the iron is substantially below the plane with a C=C–N(2)–Fe torsion angle of around 16º, compared to the much more planar conformation of the intermediate-spin species. Between spin states, the RMS deviations of the backbones are 48–49 pm. Compared to the crystal structure of the high-spin state of the unsubstituted phenyl as R" ligand reported in Ref. 3, the main features are reproduced. The largest deviations are found for the Fe–Cl(2) bond distance, which in the crystal structure is somewhat longer, 225.5 pm, compared to our computed values of 222.1–223.5 pm with the substituted phenyl ligands. The Cl(1)–Fe–Cl(2) angle in the crystal is also slightly larger, 125.6 °, compared to the computed angles of 118.8–119.8 °. The most visible difference is the orientation of the phenyl groups, which in the crystal of ^{Cy,Ph}[*N,N*]$FeCl_2$ are much

more co-planar, leading to an overall C_s symmetry of the complex. The differences can largely be explained by crystal packing effects. The energy difference between tilted and quasi-parallel phenyl groups is small (2.4 kJ/mol with R"=PhF at 0 K without ZPE). Further, the crystal structures of several of the less well-resolved complexes also show tilted substituted phenyl groups.

For a complete, interactive view of the structures, we direct the Reader toward the electronic supplementary information, which contains the molecular geometries of the studied complexes.

Figure 1. Molecular structures of the Fe(II)-Cl_2 complexes with different substituted phenyls as R" ligands. Top: The high-spin structures of R"=PhF (green), R"=PhOMe (red), and R"=PhNMe_2 (blue) superimposed. Bottom: The high-spin (red) and intermediate-spin (multi-colour) structures of R"=PhF superimposed; the atom labels define the naming scheme used in Tables 1–3.

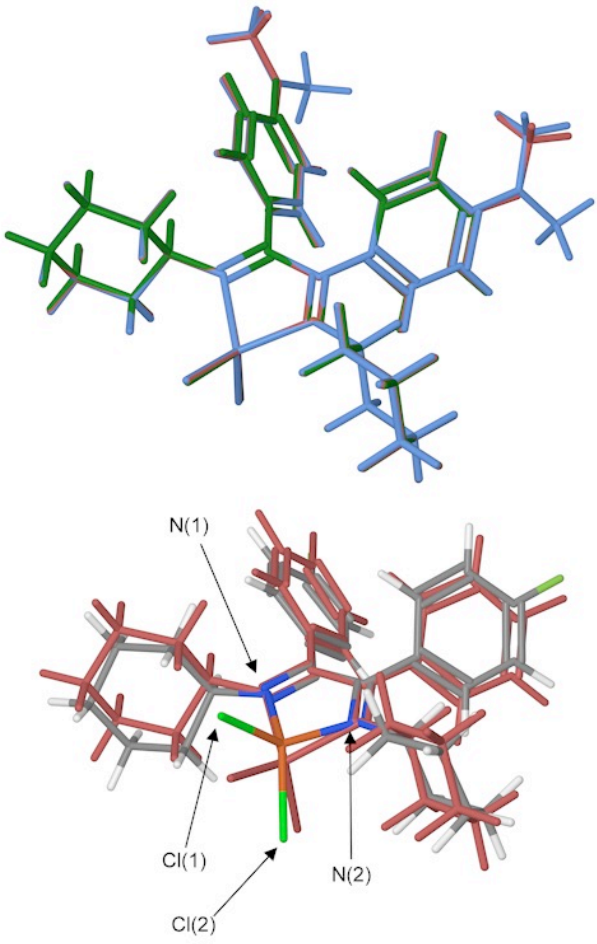

Table 1. Structural properties and relative energies for the Fe(II)-Cl_2 complexes with different substituted phenyls as R" ligands.

	R"=PhF		**R"=PhOMe**		**R"=PhNMe$_2$**	
spin state	**S=1**	**S=2**	**S=1**	**S=2**	**S=1**	**S=2**
d(Fe–Cl(1)) / pm	219.9	220.1	221.5	220.8	221.5	221.7
d(Fe–Cl(2)) / pm	219.9	222.1	221.5	222.7	221.5	223.5
<(Cl(1)–Fe–Cl(2))	107.1 °	119.8 °	106.0 °	119.5 °	106.0 °	118.8 °
d(Fe–N(1)) / pm	187.0	201.1	187.4	201.2	187.4	201.4
d(Fe–N(2)) / pm	187.0	200.7	187.4	200.8	187.4	201.0
ϕ(C–C–N(2)–Fe)	+4.4 °	-17.3 °	+5.1 °	-16.4 °	+5.1 °	-15.6 °
ΔE(0K) / kJ/mol	0	-90.4	0	-89.3	0	-89.1
ΔH(298K) / kJ/mol	0	-89.2	0	-88.3	0	-88.0
ΔG(298K) / kJ/mol	0	-93.3	0	-91.0	0	-91.6

Table 1 also shows the relative spin-state energies of the complexes. Regardless of the R" ligand, the complexes are found to be high spin. For all, the high-spin state is significantly more stable, by almost the same amount, around 90 kJ/mol. This large energy difference ensures that the starting points of the reactions, studied in Section 3.5, are the high-spin Fe(II)Cl_2 complex, with four unpaired electrons. Thermal effects have only a small impact on the relative energies. The room temperature enthalpy differences are slightly lower, and the free energy differences slightly larger than at 0 K.

3.2 Molecular and electronic structure of the Fe(III)Cl_3 ATRP complexes

Next, we consider the ATRP intermediates, where a chlorine radical is attached to the parent Fe(II) complexes, leading to the Fe(III)Cl_3 complexes. This intermediate should be favoured by the R"=PhNMe_2 complex. Table 2 summarises the main geometrical parameters and energy differences of the two spin states considered. Compared to the parent Fe(II)-Cl_2 complex, the attachment of an additional chlorine to iron effects some notable changes in the geometries. The Fe–Cl and Fe–N bonds are all elongated. Again, the bond lengths to iron are further elongated when going from intermediate to high-spin, with one exception: the Fe–N(1) bond actually shrinks very slightly. With an extra atom attached to the iron, changing the geometry from a near-tetragonal to something in-between a square pyramidal and trigonal pipyramidal conformation around iron, the Cl(1)–Fe–Cl(2) angle is naturally increased significantly. The out-of-plane character of the iron is reversed; it is now the intermediate-spin state that is more non-planar.

The differences between the same-spin structures for different phenyl substituents are slightly larger compared to the Fe(II)Cl_2 complexes, but still small. The RMS deviations for the backbones, for backwards compatibility now also excluding the third chlorine bonded to iron, are between 5.3 and 11.5 pm. Again, the difference between R"=PhF, PhNMe_2 is roughly the sum of differences of the two other pairs. The structural difference between spin states decreases significantly compared to the corresponding Fe(II)Cl_2 complexes, mainly due to a more moderate change in the out-of-plane character of Fe with changing spin state; the RMS deviations are between 10.3 and 12.3 pm.

The unpaired electron of the Cl radical can either be spin-up (α) or spin-down (β), and combining it with the four unpaired electrons of the parent Fe(II)Cl_2 complex (with S=2) can give either a high-spin Fe(III) complex with five unpaired electrons (S=5/2), or an intermediate-spin complex with three unpaired electrons (S=3/2). From Table 2 we see that, again, all three complexes clearly favour the high-spin state, although to a lesser degree than for the parent complexes. Compared to the Fe(II)-Cl_2 complexes, the differences caused by the R" ligands are, however, growing larger. With PhF, which should follow an (intermediate-spin) CCT pathway, the free energy

spin-state splitting is the lowest. The PhOMe R" ligand favours high-spin slightly more, and the $PhNMe_2$ ligand, which should follow this high-spin ATRP route, has a spin-state splitting of 6.2 kJ/mol more in favour of high-spin compared to PhF. Thus, there is a systematic trend, which qualitatively agrees with the observation that $PhNMe_2$ should follow the ATRP pathway *via* this intermediate.

Table 2. Structural properties and relative energies for the Fe(III)-Cl_3 complexes with different substituted phenyls as R" ligands.

	R"=PhF		**R"=PhOMe**		**R"=$PhNMe_2$**	
spin state	**S=3/2**	**S=5/2**	**S=3/2**	**S=5/2**	**S=3/2**	**S=5/2**
d(Fe–Cl(1)) / pm	223.6	228.3	224.2	229.3	225.4	230.9
d(Fe–Cl(2)) / pm	222.9	228.5	223.2	229.3	224.4	231.3
<(Cl(1)–Fe–Cl(2))	162.9 °	151.0 °	162.7 °	152.3 °	161.5 °	152.4 °
d(Fe–N(1)) / pm	211.0	210.9	210.8	209.7	209.6	207.5
d(Fe–N(2)) / pm	198.2	222.7	198.2	220.8	197.5	218.3
ϕ(C–C–N(2)–Fe)	-10.3 °	-6.4 °	-9.2 °	-4.9 °	-8.4 °	-4.2 °
d(Fe–Cl(3)) / pm	222.3	226.6	223.1	227.4	224.3	228.6
ΔE(0K) / kJ/mol	0	-42.6	0	-43.9	0	-46.8
ΔH(298K) / kJ/mol	0	-41.5	0	-42.9	0	-45.5
ΔG(298K) / kJ/mol	0	-46.4	0	-47.5	0	-52.6

3.3 Disproportionation of the Fe(III)Cl_3 complexes

The magnetic-moment measurements by Allan *et al.*[3] indicated that with electron-withdrawing R" groups, including R"=PhF, PhMeO, the Fe(III)-Cl_3 complexes were found in an intermediate-spin state, and only R"=$PhNMe_2$ in a high-spin state. We find it highly unlikely that the computations would be in error by 50 kJ/mol, so this discrepancy is slightly puzzling. The calculations rule out a

possible mixture of high- and low-spin states as the explanation; the S=1/2 states of the three complexes are all 70-80 kJ/mol above the high-spin ground state. In the calculations, the solvent is treated implicitly by the means of a continuum model. That an explicit interaction with solvent molecules would lead to a difference so strikingly different for the three complexes would be very surprising, however. Instead, it is likely that, with electron withdrawing groups, the Fe(III)-Cl_3 complexes are not stable enough to survive in solution, thus rendering the experimentally derived spin states questionable. This was noted already in Ref. 3, where attempts at crystallising the proposed intermediate-spin complexes failed, and lead to disproportionation of the complexes, with a loss of the $FeCl_3$ group. Specifically, the attempted crystallisation of $^{tBu,PhF}[N,N]FeCl_3$ showed that two of the Fe(III)Cl_3 complexes had disproportionated as follows (note the additional hydrogen on the right hand side):

$$2\ ^{tBu,PhF}[N,N]FeCl_3 \rightarrow {}^{tBu,PhF}[N,N]FeCl_2 + FeCl_4^- + {}^{tBu,PhF}[N,N]H^+$$

Allan *et al*. also note that it was not possible to obtain meaningful ^1H NMR spectra of the Fe(III)Cl_3 complexes.[3] If disproportionation occurs also in solution, even partly, the presence of organic low-spin radicals would lower the measured magnetic moments. In order to check the viability of disproportionation in solution, we now consider the following disproportionation reactions computationally:

(a) $2\ ^{Cy,R"}[N,N]FeCl_3 \rightarrow {}^{Cy,R"}[N,N]FeCl_2 + FeCl_4 + {}^{Cy,R"}[N,N]$
S=5/2 *S=2* *S=2* *S=0*
Only neutral species produced

(b) $2\ ^{Cy,R"}[N,N]FeCl_3 \rightarrow [{}^{Cy,R"}[N,N]FeCl_2^+ + FeCl_4^-] + {}^{Cy,R"}[N,N]$
S=5/2 *S=5 (5/2+5/2)* *S=0*
Two charged, ferromagnetically coupled Fe complexes produced

(c) $2\ ^{Cy,R"}[N,N]FeCl_3 \rightarrow {}^{Cy,R"}[N,N]FeCl_2 + [FeCl_4^- + {}^{Cy,R"}[N,N]^{+*}]$
S=5/2 *S=2* *S=2 (5/2 – 1/2)*
Charged organic radical antiferromagnetically coupled to $FeCl_4^-$

(d) $2\ ^{Cy,R"}[N,N]FeCl_3 + CHCl_3 \rightarrow {}^{Cy,R"}[N,N]FeCl_2 + [FeCl_4^- + {}^{Cy,R"}[N,N]H^+] + CCl_3{}^*$
S=5/2 *S=0* *S=2* *S=5/2 (5/2 + 0)* *S=1/2*
Reaction (c) coupled with hydrogen abstraction from solvent (chloroform)

Reaction (d) corresponds to the disproportionation observed in the crystal structure, emphasising that in order for the organic, closed-shell $^{Cy,R''}[N,N]H^+$ cation to form, hydrogen abstraction, here from the solvent, is necessary.

Table 3. Reaction energies for the disproportionation reactions (a)—(d). Values in kJ/mol. Also shown is the average spin-only magnetic moment per paramagnetic centre of the products (μ_{avg}).

		R''=PhF	R''=PhOMe	R''=PhNMe$_2$	μ_{avg}
reaction (a)	**ΔE(0K)**	+209.0	+213.3	+211.6	4.90
	ΔH(298K)	+204.2	+208.7	+206.1	
	ΔG(298K)	+155.2	+157.5	+161.1	
reaction (b)	**ΔE(0K)**	-2.2	-1.3	-33.2	5.92
	ΔH(298K)	-1.6	-0.7	-33.7	
	ΔG(298K)	-3.9	-3.9	-33.0	
reaction (c)	**ΔE(0K)**	+96.4	+79.5	+5.6	4.18
	ΔH(298K)	+98.6	+81.9	+4.9	
	ΔG(298K)	+90.0	+70.8	+13.2	
reaction (d)	**ΔE(0K)**	+25.9	+18.9	+10.0	4.18
	ΔH(298K)	+26.7	+19.9	+8.0	
	ΔG(298K)	+24.4	+15.8	+16.4	

Table 3 shows the reaction energies for the four considered disproportionations. For the reactions (b)—(d) where the anionic Fe(III)Cl_4^- species is produced and coupled with the cationic species, the structures have been fully relaxed to the closest stable minima on the potential energy surface, with the starting point of the optimisation based on the crystal structure of the disproportionated $^{tBu,PhF}[N,N]FeCl_3$ complex (ID RIRJIM).[3] Specifically, a thorough sampling of all the possible relative geometries between anion and cation in the supercomplex has *not* been

performed. Further, with a loss of the iron atom coordinated to the two nitrogens in the $^{Cy,R"}[N,N]$ complexes, the resulting organic species becomes quite flexible, with rotation of the NC—CN bond relatively unhindered. Thus, the reaction energies are probably somewhat too endothermic, and should be considered qualitative, rather than quantitative. For elucidating the effect of the R" group on the relative energies, they serve their purpose sufficiently well, however.

It is evident that reaction (a) is not favourable, and can be ignored. Reaction (b), on the other hand, is exothermic; barely so with the electron-withdrawing R" groups PhF and PhOMe, but quite significantly with the electron-donating R"=PhNMe$_2$. This qualitative difference can be explained by the interaction with the $FeCl_4^-$ anion, located in the proximity of the R" ligands: The electron-donating R"=PhNMe$_2$ groups form a much more favourable interaction with the anion, compared to the already slightly negative electron-withdrawing R" groups.

An even larger qualitative difference is observed for reaction (c), where the electron-withdrawing R" groups render the reaction unviable, while the electron-donating R"=PhNMe$_2$ group again lowers the reaction energy significantly, making the disproportionated product practically isoenergetic with the parent Fe(III)Cl$_3$ complex. Again, the qualitative difference can be traced to the electrostatic interaction between the R" groups and the $FeCl_4^-$ anion.

Finally, we consider reaction (d), where reaction (c) is coupled to hydrogen abstraction from the solvent. With R"=PhF, PhOMe, hydrogen abstraction significantly lowers the reaction energy. With R"=PhNMe$_2$, on the other hand, hydrogen abstraction is not favourable. This significant difference between the complexes with electron-withdrawing and donating character can be traced to the spin-density distribution of the $^{Cy,R"}[N,N]^{+*}$ radical cation. With R"=PhF, the unpaired electron is strongly located around the two nitrogens that "normally" are coordinated to the iron, with a combined Mulliken spin population of 0.76 *e*. With R"=PhOMe, the spin is more delocalised, spreading out onto the phenyl rings, and the spin population of the nitrogens falls to 0.41 *e*. With the electron-donating R"=PhNMe2, these two nitrogens are almost closed-shell, with a combined spin-population of only 0.04 *e*; the spin has almost completely migrated out to the phenyl ring and the -NMe$_2$ groups. Figure 2 shows the spin distribution of the three complexes. Thus, the process where

one of the nitrogens captures a hydrogen from the solvent in order to make the complex closed-shell becomes decreasingly less favourable with decreasing unpaired spin on the nitrogens: ΔΔG(298K) between reactions (c) and (d) rises from -65.6 kJ/mol with R"=PhF *via* -55.0 kJ/mol with R"=PhOMe to being endergonic by +3.2 with R"=$PhNMe_2$.

Figure 2. Structures and spin densities of the [$^{R"}$[*N,N*]$^{+\bullet}$ + $FeCl_4^-$] complexes. Dark blue shows regions with excess α-spin density, light red shows excess β-spin density.

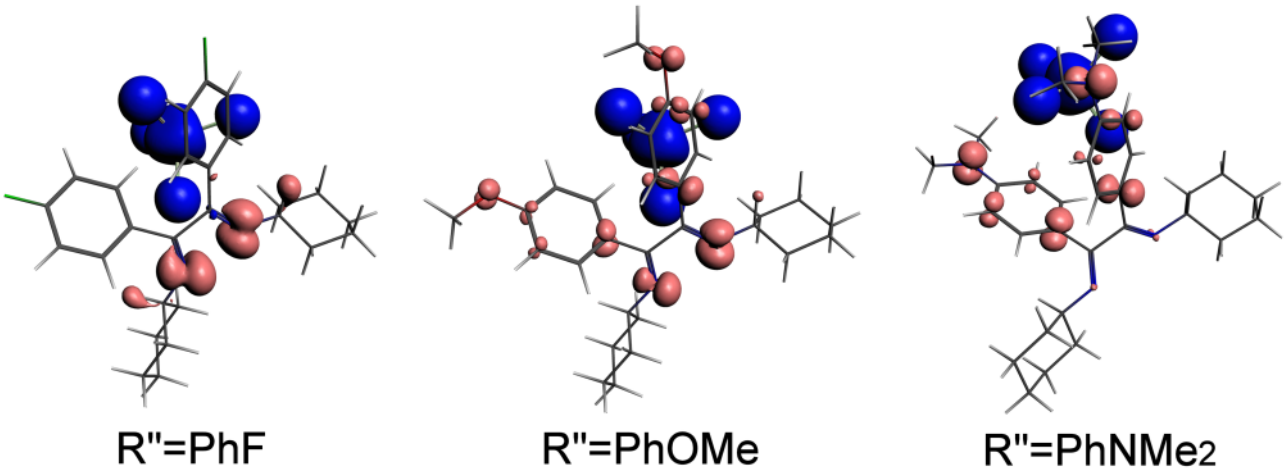

Combined, the reaction energies presented in this section, and the relative spin state energies of the previous section provide a resolution to the apparent discrepancy between the computed spin states of the Fe(III)Cl_3 complexes and the experimental magnetic-moment measurements. In the case of the electron-donating R"=$PhNMe_2$ complex, disproportionation reaction (b) is clearly the most likely. The average spin-only magnetic moment of the products of this reaction is the same as that of the original Fe(III)Cl_3 species, 5.92 μ_B, in agreement with the measurements in Ref [3]. Also with R"=PhF, PhOMe, reaction (b) is computed to be the most favourable, although to a much lesser degree than when R"=$PhNMe_2$. The disproportionation reaction (d), which gives an average spin-only magnetic moment of 4.18 μ_B compared with the measured magnetic moments of 3.9-4.2 μ_B for the complexes with electron-withdrawing R" groups, is only slightly less favourable. With the noted caveat of the computed reaction energies being somewhat too positive, we believe that the data strongly suggests that disproportionation indeed takes place in solution, and that the magnetic

moments measured are not those of the high-spin Fe(III)Cl_3 species, but instead of the disproportionated products, as suggested by the experimental crystal structure. Further, as will be shown below, the selectivity of specific R" ligands towards the two competing polymerisation pathways can be accounted for even without varying spin states for the Fe(III)-Cl_3 complexes.

3.4 Molecular and electronic structure of the Fe(III)Cl_2-Bn CCT complexes

The third case we study is the Fe(III) intermediate of the CCT pathway, where the parent Fe(II)-Cl_2 complex is attached to the benzyl radical (Bn*), instead of Cl*, producing the Fe(III)-Cl_2-Bn complexes. Figure 3 shows the structure of the resulting complex, using R"=PhF as an example. The structural properties and spin-state splittings for these complexes are tabulated in Table 4. Upon attachment of the benzyl radical, we can again observe a notable elongation of the Fe–Cl and Fe–N bonds, compared to the same-spin Fe(II)Cl_2 parent complex. The overall geometry around iron is closer to an ideal trigonal pipyramidal structure, compared to the Fe(III)-Cl_3 complexes. Compared to the high-spin parent complex, the iron is more planar with respect to the diimine ring system. The geometrical differences between spin states are also notable. In these complexes, the largest change is seen in the Fe–Cl bonds and the Fe–C bond to benzyl. The RMS deviation analysis reveals qualitatively the same trend as for the two other complex families discussed above. With the same spin state, the differences are moderately small, between 3.5 and 10.6 pm, the biggest difference seen between the high-spin R"=PhF, $PhNMe_2$ pair. Between spin states, the RMS difference is slightly larger, 12.9–14.4 pm. This is on the same order as that of the Fe(III)-Cl_3 complexes, and much smaller than for the Fe(II)-Cl_2 species, again due to the quite small change in out-of-plane character of iron between spin states.

Looking at the spin state energetics, we see a qualitative change. The intermediate-spin state is now energetically favoured over the high-spin state. With R"=PhF, PhOMe, the difference is the largest, consistent with the observation that with these ligands, polymerisation follows an intermediate-spin CCT mechanism. For the R"=$PhNMe_2$ Fe(III)-Cl_2-Bn complex, the free energy difference is more modest, being only 13.7 kJ/mol. But again, all three ligands are qualitatively

identical, favouring intermediate spin. For completeness, we again ruled out the possibility of the low-spin state being even more stable; the S=1/2 states are around 40 kJ/mol higher in energy than the S=3/2 states. We note that the pacifier-shaped, σ-type spin-polarisation, typical for low- and intermediate-spin iron complexes,[32,55,56], can be observed along the Fe–C bond in Figure 3.

Figure 3. Structure and spin density of the $^{R"}$[*N,N*]FeCl$_2$-Bn, R"=PhF complex. Dark blue shows regions with excess α-spin density, light red shows excess β-spin density.

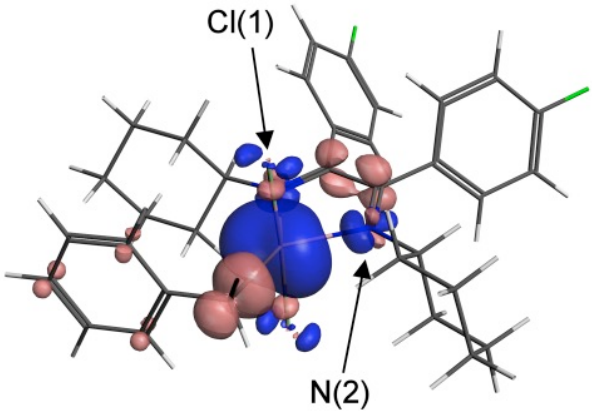

Table 4. Structural properties and relative energies for the Fe(III)-Cl$_2$-Bn complexes with different substituted phenyls as R" ligands.

	R"=PhF		**R"=PhOMe**		**R"=PhNMe$_2$**	
spin state	**S=3/2**	**S=5/2**	**S=3/2**	**S=5/2**	**S=3/2**	**S=5/2**
d(Fe–Cl(1)) / pm	227.3	237.5	227.7	238.5	228.1	240.3
d(Fe–Cl(2)) / pm	227.3	234.3	227.4	234.9	227.7	236.0
<(Cl(1)–Fe–Cl(2))	175.2	176.1	175.2	176.8	175.2	177.9
d(Fe–N(1)) / pm	203.9	213.8	203.9	212.6	203.6	210.5
d(Fe–N(2)) / pm	205.3	209.9	205.4	208.8	205.4	207.3
ϕ(C–C–N(2)–Fe)	+6.0	+4.3	+5.7	+4.6	+5.9	+6.0
d(Fe–C(Bn)) / pm	206.6	215.7	206.5	215.9	206.3	216.1
ΔE(0K) / kJ/mol	0	+29.6	0	+26.4	0	+20.7
ΔH(298K) / kJ/mol	0	+31.2	0	+27.8	0	+22.5

ΔG(298K) / kJ/mol	0	+25.5	0	+22.5	0	+13.7

The results of this and the preceding two sections thus show that even if the trends in spin state energies of the Fe(III) intermediates agree with the trend for favouring either ATRP or CCT, they do not as such differentiate between the two pathways. All species, the parent Fe(II)-Cl_2, the ATRP intermediate Fe(III)-Cl_3, and the CCT intermediate Fe(III)-Cl_2-Bn possess the same spin-state, either high or intermediate-spin, regardless of the nature of the R" phenyl ligand. To explain the pathway selection induced by varying the ligand, we need to consider the full reaction energetics of this first step of polymerisation.

3.5 Reaction energies

In this section, we analyse the reaction energies of the model ATRP and CCT reactions with benzyl chloride, shown in Scheme 1. Based on the spin-state splittings of the previous section, we note that only two reactions need to be considered: (1) the ATRP reactions, starting from the high-spin Fe(II)-Cl_2 complexes and producing the high-spin Fe(III)-Cl_3 complexes; (2) the CCT reactions, also starting from the high-spin Fe(II)-Cl_2 complexes and producing the intermediate-spin Fe(III)-Cl_2-Bn complexes. For the CCT reactions, we study two cases, where the Cl* radical detached from BnCl either recombines with another Cl* radical (2a) or partakes in hydrogen abstraction from the solvent, chloroform (2b):

(1) ATRP $\quad BnCl + {}^{R"}[N,N]Fe(II)Cl_2, S=2 \rightarrow Bn^* + {}^{R"}[N,N]Fe(III)Cl_3, S=5/2$

(2a) CCT $\quad BnCl + {}^{R"}[N,N]Fe(II)Cl_2, S=2 \rightarrow \frac{1}{2}Cl_2 + {}^{R"}[N,N]Fe(III)Cl_2\text{-}Bn, S=3/2$

(2b) CCT $\quad BnCl + CHCl_3 + {}^{R"}[N,N]Fe(II)Cl_2, S=2$

$$\rightarrow HCl + CCl_3^* + {}^{R"}[N,N]Fe(III)Cl_2\text{-}Bn, S=3/2$$

[*N*,*N*] = Cy-N=CR"-CR"=N-Cy

R" = PhF, PhOMe, $PhNMe_2$

Cy = cyclohexyl

BnCl = benzyl chloride, $C_6H_5CH_2Cl$

$CHCl_3$ = chloroform

For clarity, we note that the nomenclature for the CCT reaction can be somewhat misleading. Even if the spin-state of the iron complex during the reaction changes from high to intermediate spin, no spin-flips take place. The number of unpaired electrons changes by one in both the ATRP and CCT reactions, and depends on the spin, α or β, of the attaching radical.

Table 5 summarises the reaction energies for reactions (1) and (2), showing the reaction energy at absolute zero, both with and without ZPE, as well as the reaction enthalpy (ΔH) and free energy (ΔG) at room temperature. All reactions are uphill, endothermic and endergonic, as expected. For the ATRP reactions, the ZPE has a large, favourable effect on the reaction energies. For the CCT reactions (2a), it is the free energy corrections that are substantial, and the entropy contributions significantly increase the endergonicities at room temperature. For the hydrogen abstraction model of the CCT reactions (2b), a competition between both effects can be seen: ZPE lowers the endothermicity, while entropy contributions are stronger, again increasing endergonicity. The fraction of reactions that would follow the ATRP reaction path, according to the different computed relative energies between the ATRP (1) and CCT (2a) reactions, are also shown. These are computed from a simple Boltzmann distribution:

$$\%\,\mathrm{ATRP} = \frac{100}{1 + e^{-\Delta(\mathrm{ATRP,CCT})/(k_b T)}}$$

Table 5. Reaction energies for the ATRP (1) and CCT (2) reactions, as well as differences between the R"=PhF and R"=$PhNMe_2$ energetics. Values in kJ/mol. The fraction of reactions proceeding *via* the ATRP mechanism (1) compared to the CCT mechanism (2a), based on the computed relative energies, is also shown.

		R"=PhF	**R"=PhOMe**	**R"=$PhNMe_2$**	***Δ(R"=PhF, $PhNMe_2$)***
reaction (1) ATRP	**ΔE(no ZPE)**	122.9	120.9	118.9	*-4.0*
	ΔE(0K)	115.2	113.3	110.8	*-4.4*
	ΔH(298K)	117.0	115.1	112.9	*-4.1*
	ΔG(298K)	116.9	115.4	110.8	*-6.1*
reaction (2a) CCT	**ΔE(no ZPE)**	123.5	124.6	130.4	*+6.9*
	ΔE(0K)	125.4	126.4	132.3	*+6.9*
	ΔH(298K)	126.7	127.7	133.5	*+6.8*
	ΔG(298K)	168.1	168.7	175.5	*+7.4*
reaction (2b) CCT	**ΔE(no ZPE)**	200.2	201.3	207.0	*+6.9*
	ΔE(0K)	186.0	187.0	192.9	*+6.9*
	ΔH(298K)	190.1	191.1	196.9	*+6.8*
	ΔG(298K)	209.0	209.5	216.3	*+7.4*
Δ(ATRP, CCT) (% ATRP)	**ΔΔE (no ZPE)**	+0.6 (56%)	+3.7 (82%)	+11.4 (99%)	*+10.8*
	ΔΔE(0K)	+10.2 (98%)	+13.1 (99%)	+21.5 (100%)	*+11.3*
	ΔΔH(298K)	+9.7 (98%)	+12.7 (99%)	+20.6 (100%)	*+10.9*
	ΔΔG(298K)	+51.2 (100%)	+53.3 (100%)	+64.7 (100%)	*+13.5*

We can see that, according to the computed reaction energies, the ATRP pathway is consistently favoured over the CCT reactions. Ideally, there should be a qualitative difference for the pathway energetics depending on the R" ligand, with R"=PhF, PhOMe encountering a smaller reaction barrier when following the CCT pathway, and only R"=$PhNMe_2$ facing a gentler uphill slope by taking the ATRP route. The energy differences are very small however, at least when entropic effects are neglected. Let us first consider the R"=PhF case, which should follow a CCT reaction path. The electronic energy difference between the CCT (2a) and ATRP reactions is very small, only 0.6 kJ/mol. When ZPE is added, the difference increases to 10.2 kJ/mol, and is slightly decreased, to 9.7 kJ/mol, when looking at the room temperature reaction enthalpy. When the R" group is exchanged for PhOMe, the ATRP reaction becomes even more favourable. And, as should be the case, for R"=$PhNMe_2$, the ATRP reaction is favoured most strongly.

What is encouraging is that the calculations reproduce the expected trend perfectly; the energies of the reactions with R"=PhOMe fall in between those of R"=PhF and $PhNMe_2$, but are much closer to those of R"=PhF, in agreement with the experimentally observed behaviour. The absolute reaction energies of the first steps of the catalytic cycles do not by themselves fully explain the differentiation, however. If the room temperature enthalpies of the CCT (2a) reactions were lowered by just 12.8 kJ/mol (or alternatively, the ATRP reaction enthalpies were increased by the same amount, or any combination of the two) the energy orders of the competing reactions would be in accord with the experimentally observed behaviour. This is quite a small "error", considering the simplifications and approximations used in computing the energies, for example, modelling the solvent only implicitly, and basing the thermal corrections on only the vibrational frequencies, computed within the harmonic approximation for gas-phase species.[48]

If we look at the Gibbs free energies, ΔG, which have been found to be more important for the reactions of transition metal complexes,[57] we see an increased discrepancy. The trend in reaction free energies is still correct, with ATRP increasingly more favourable in the series R"=PhF, PhOMe, $PhNMe_2$. With R"=PhNMe2, the difference between the ATRP and CCT pathways is 13.5 kJ/mol larger compared to the R"=PhF reaction pair. The ATRP reaction free energy is, however, 51.2

kJ/mol lower than the CCT (2a) free energy even for R"=PhF. To get an energy order consistent with observed behaviour, the computed relative free energies would have to be in error by at least 53.4 kJ/mol, with the assumption that it is the free energies of this first step of the catalytic reaction that is the deciding factor. While we cannot categorically rule out such a large error in the computed energies, we find it to be highly unlikely. Instead, it would probably be necessary to consider how the different reactions proceed *after* the initial steps studied here. An indication of this is, as we will see in the next section, that entropic effects break the benzyl—iron bond. Also the transition states could provide additional insight of the selectivity. Already the initial steps *do* show clear differences in the reaction energies with varying R" ligands that are consistent with observations, and without a direct relation to the spin states of the intermediate species, however. This suggests that the underlying reason for differentiation lies in small, accumulating energetic effects, instead of being directly related to the spin state of iron. In the next section, we inspect these subtle effects in more detail.

3.6 Origins of the pathway differentiation

We finish with an attempt at explaining how the distant phenyl substituent is able to so dramatically change the reaction behaviour around the iron centre. The electronic character of the substituents immediately suggests electrostatics as a candidate for differentiation. The bond path from the phenyl substituent to iron is more or less conjugated all the way. Thus, an electron withdrawing or donating behaviour of the R" ligand could potentially change the charge distribution around the metal. A look at the atomic charges reveals that this is indeed the case. The Hirshfeld charge[58] of iron in the parent Fe(II)-Cl_2 complexes evolves with changing electron affinity of the phenyl ligands in the expected order, being +0.23, +0.22 and +0.20 for R"=PhF, PhOMe and $PhNMe_2$, respectively. The differences are small, but clear. If we look at the sum of the atomic charges of the –$FeCl_2$ group, we observe the same trend; the total charge of the three atoms are –0.40, –0.43 and –0.50 for the three R" groups, respectively.

The electrostatic potential (ESP) paints a perhaps more directly physical picture. Figure 4 shows the ESP for R"=PhF and R"=PhNMe$_2$. For a prospecting, electron hungry Cl radical, awaiting to follow the ATRP pathway, the R"=PhNMe$_2$ complex presents a much more appetising front. Transversely, the less negative –FeCl$_2$ group of the complexes with electron withdrawing ligands would then be favoured by the organic radical attaching *via* the CCT mechanism. Small electronic interaction differences are thus seen to be intimately related to the two different pathways.

Figure 4. The electrostatic potential (ESP) plotted on an isosurface of the charge density for the R"=PhF (left) and R"=PhNMe$_2$ (right) complexes. The colour scale shows the magnitude of the ESP in different regions of the molecules.

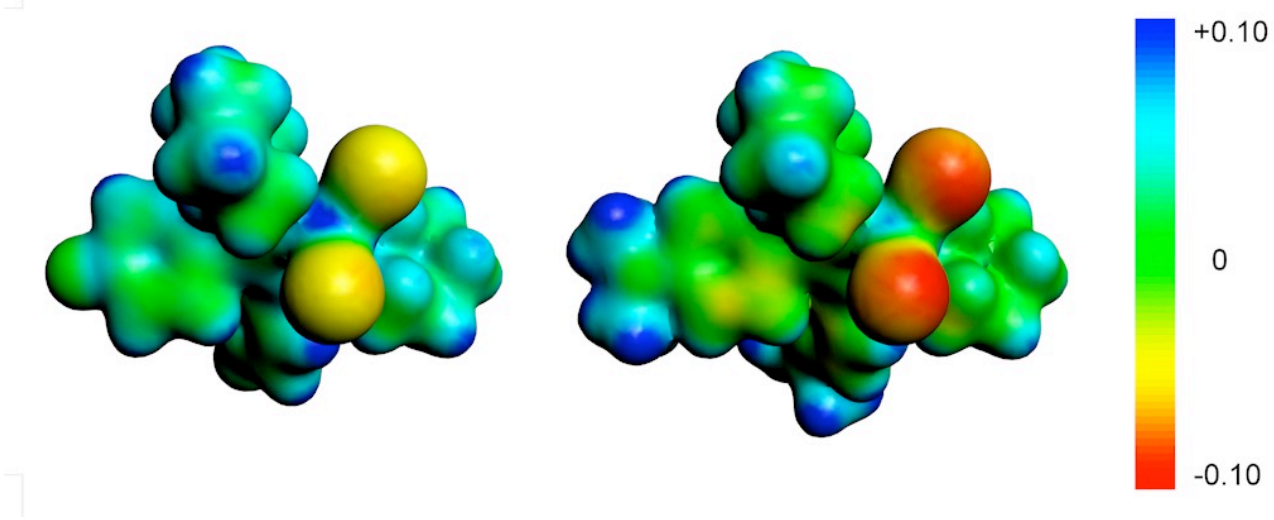

Another subtle difference between the parent Fe(II)Cl$_2$ complexes favouring either the chlorine or benzyl radical as a fifth ligand to iron comes from the reorganisation energy (λ) upon bonding. We borrow the concept from its more familiar setting of electron transfer theory,[59] noting that it has proven potential to provide insight also for normal reactions.[60,61] Here, we define the reorganisation energy as the energy difference of the unbound species in their optimal, optimised geometry and that of the geometry they assume after completed bonding. While the qualitative character of the electrostatic effect discussed above could be predicted *a priori*, providing even an educated guess of the effect of the reorganisation energy in this context is difficult. Table 6 shows the bonding energies and λ's for the reactions considered. The bonding energies without zero-point

vibrational energy correction are also reported, for more directly comparable differences against reorganisation energies, as they too are computed without any thermal corrections. For the bonding energetics, we have used the free Cl radical.

The bond energies necessarily show the same energy order as the total reaction energies, discussed in the previous sections. Table 6 emphasises the crucial importance of accounting for thermal corrections more clearly, however. Entropic effects influence the energies significantly. Especially dramatic is the effect on the Fe(III)Cl_2-Bn CCT intermediate; at 298 K, the bonding energy of the benzyl radical to the Fe(II)Cl_2 complex is positive! That is, for all species, the benzyl would not be bound at all, being unfavourable by 0.5 kJ/mol for R"=PhF, to 7.8 kJ/mol with R=PhNMe_2. This clearly illustrates the fleeting character of this intermediate, which is corroborated by the fact that no crystal structures are present in the Cambridge crystal structure database with an iron-carbon bond in these Fe(III)-Cl_2N_2C complexes. For R"=PhNMe_2, it is possible that this intermediate could not be formed at all, which would effectively prevent the CCT pathway altogether for this complex. It also suggests an immediate procession of the CCT reaction, and could possibly explain the large difference in reaction free energies in favour of the ATRP pathway at this first stage of the process, as discussed in the previous section. For the CCT intermediate, the strongest bond is formed when R"=PhF, PhOMe, while the ATRP intermediate complex forms the strongest bond when R"=PhNMe_2.

A large part of the difference in bonding energies comes from the differences in reorganisation energy. For the ATRP intermediate, the R"=PhNMe_2 Fe(II)-Cl_2 complex is distorted the least, as measured by the ensuing energy penalty. Of the total bonding energy difference (at absolute zero without ZPE) between R"=PhF and R"=PhNMe_2 half can be attributed to the reduced need for geometry distortion.

For the CCT intermediates, the situation is reversed. In general, the reorganisation energies are much larger than for the ATRP intermediates. Here, it is the R"=PhF Fe(II)-Cl_2 complex that undergoes the least change. Further, also the benzyl radical ligand undergoes a smaller change upon attachment to the complexes with electron withdrawing groups. In this case, the differences in λ

accounts for a crucial part of the differences in bonding energy. The total difference in favour of R"=PhF over R"=PhNMe$_2$ without thermal corrections is 6.9 kJ/mol, whereas the difference in reorganisation energy is 1.4 times larger than this, 9.7 kJ/mol. That is, were the reorganisation energy equal for the three species, the bonding energy order would actually be reversed!

Table 6. Bond energies for the fifth ligand to iron, Cl* (ATRP) or Bn* (CCT), the reorganisation energies (λ) for the parent Fe(II)Cl$_2$ complex and the benzyl radical (Bn*). Values in kJ/mol.

		R"=PhF	**R"=PhOMe**	**R"=PhNMe$_2$**	***Δ(R"=PhF, PhNMe$_2$)***
Reaction (1) ATRP	**ΔE_b(no ZPE)**	-214.3	-216.3	-218.3	*-4.0*
	ΔE_b(0 K)	-210.4	-212.3	-214.8	*-4.4*
	ΔH_b(298 K)	-211.3	-213.3	-215.5	*-4.2*
	ΔG_b(298 K)	-178.6	-180.1	-184.7	*-6.1*
	λ (Fe(II)Cl$_2$)	74.6	75.5	72.5	*-2.1*
Reaction (2a) CCT	**ΔE_b(no ZPE)**	-72.0	-70.9	-65.1	*+6.9*
	ΔE_b(0 K)	-60.1	-59.1	-53.1	*+7.0*
	ΔH_b(298 K)	-58.7	-57.6	-51.9	*+6.8*
	ΔG_b(298 K)	+0.5	+1.0	+7.8	*+7.3*
	λ (Fe(II)Cl$_2$)	89.3	91.2	97.8	*+8.5*
	λ (Bn*)	21.6	22.2	22.8	*+1.2*
	λ (total)	110.9	113.4	120.6	*+9.7*

This analysis shows that the energetic difference between the ATRP and CCT reactions for the different phenyl substituents comes from two relatively minor effects:

1. The electrostatic interaction of the iron centre with a chlorine radical is enhanced by an electron-donating R" group, which favours the ATRP pathway, and *vice versa*, an electron-withdrawing R" group favours an interaction with an organic radical, leading to the CCT intermediate.
2. The structure of the parent complex and the attaching ligand undergo a smaller change, energetically, when the CCT intermediate is formed with an electron donating group compared to an electron withdrawing group, and *vice versa* for the ATRP intermediate.

Together, the effects accumulate, and disregarding entropy, *almost* sufficiently to lead to either ATRP or CCT being favoured, depending on the character of the phenyl substituent. This agrees with the experimentally observed behaviour, but at the same time suggests that the underlying reasons are more complex than merely a difference in spin state of iron.

3.7 Effects of functional and basis set size

Although spin-state energies were among the main properties that the SSB-D functional was developed for, one cannot categorically rule out the possibility that some species would be exceptionally problematic and thus poorly described at SSB-D level. Therefore, it is of interest to assess how more established functionals perform for the systems studied here. "Pure" generalised gradient approximation (GGA)[62] functionals, without exact exchange, tend to artificially favour lower spin states. On the other hand, hybrid functionals that include Hartree–Fock type exchange artificially favour higher spin states. The HF description only considers the Fermi-correlation between like spins, completely ignoring the correlation between electrons of different spins. As the exchange interaction between electrons with parallel spins is attractive, the higher the spin, the lower the HF energy, in accordance with Hund's rules,[63] leading to overstabilisation of high-spin states. In this section, we report the electronic energies of the studied iron complexes computed at BP86-D

level, expected to favour lower spin, and B3LYP-D level,[64,65] expected to favour higher spin. In addition, we have used the B3LYP* functional,[66] which uses 15% HF exchange instead of the standard 20% in B3LYP. This was shown to significantly improve LS/HS energy splitting for Fe(II) complexes.[66] In addition to the effect of the density functional used, we have also checked the basis set requirements for reliable spin state energies, by employing both triple-zeta and quadruple-zeta basis sets. Table 7 summarises the energy differences between the intermediate and high-spin configurations at the different levels of theory.

Table 7. Electronic energy differences between the high and intermediate-spin species with different functionals, using triple-zeta (TZ) and quadruple-zeta (QZ) basis sets on the BP86-D optimised structures. TZP, TZ2P, and QZ4P Slater-type basis sets[46] were used for SSB-D, def2-TZVP and def2-QZVPP Gaussian-type basis sets[41] for the other functionals. Negative values indicate that the HS complex is more stable. Energies in kJ/mol.

	ΔE(high spin/intermediate spin)						
complex	SSB-D / TZP	SSB-D / TZ2P	SSB-D / QZ4P	BP86-D / TZVP	BP86-D / QZVPP	B3LYP-D / TZVP	B3LYP* / TZVP
$Fe(II)Cl_2$							
R"=PhF	-76.7	-74.8	-88.1	-30.0	-30.9	-87.6	-75.2
R"=PhOMe	-76.8	-74.8	-87.5	-30.9	-31.8	-90.0	-77.0
R"=$PhNMe_2$	-78.3	-76.4	-87.0	-32.6	-33.7	-93.2	-79.8
$Fe(III)Cl_3$							
R"=PhF	-45.3	-40.7	-41.2	+5.8	+6.3	-31.3	-23.5
R"=PhOMe	-45.3	-40.9	-42.5	+5.3	+5.9	-30.0	-21.9
R"=$PhNMe_2$	-46.8	-42.9	-44.6	+3.6	+4.1	-29.6	-21.6
$Fe(III)Cl_2$-Bn							
R"=PhF	+16.7	+19.9	+33.2	+53.7	+53.2	+5.8	+19.3
R"=PhOMe	+13.2	+16.3	+29.7	+50.2	+49.6	+5.7	+18.4
R"=$PhNMe_2$	+7.4	+10.4	+24.4	+44.7	+44.0	+4.7	+15.9

The results corroborate and confirm the conclusions drawn from the SSB-D calculations. In general, the SSB-D energies fall between those of BP86-D and B3LYP-D, and are close to the B3LYP* splittings. The largest differences are observed for the Fe(IIII)Cl_3 species. Importantly, the functionals agree on the stability order of the complexes in different spin states, the only exception being the Fe(III)Cl_3 complexes, where BP86-D very slightly favours the intermediate spin state. This fits the well-known tendency of BP86 to underestimate the stability of high-spin complexes.

It is also evident that a standard basis set of triple-zeta quality is not always sufficient for obtaining converged spin-state energies. The relative differences are up to 17 kJ/mol for SSB-D/TZP and SSB-D/QZ4P. A significant sensitivity toward basis set size for relative spin state energies in iron complexes, especially for high-spin states, has been noted before.[67] The BP86-D results, obtained with the Gaussian-type def2-TZVP and def2-QZVPP basis sets, exhibit a much more moderate basis set sensitivity, however.

4. Summary and conclusions

We have studied a family of reactions of α-diimine iron complexes, with the general formula $^{R',R''}$[*N*,*N*]$FeCl_2$ ($^{R',R''}$[*N*,*N*] = R'–N=CR''–CR''=N–R'), using high-level quantum chemical methodology. These complexes have previously been found to follow two different polymerisation pathways, either ATRP or CCT, depending on the nature of the R' and R'' ligands.[1-4] We showed that contrary to what was suggested, the ligands do not control the spin-state of the complexes. Instead, electron-withdrawing and electron-donating R'' groups adjust the relative energies of the ATRP and CCT pathways differently, by subtle charge-transfer effects that propagate all the way to the iron, more than 8 Å away. Further, the need for structural reorganisation upon formation of the intermediate complexes enhances this effect. Formation of the Fe(III)Cl_3 ATRP intermediate carries a smaller energy penalty for the parent complex with an electron donating R'' group, compared to electron-withdrawing R'' groups. Conversely, the reorganisation energy associated with the Fe(III)Cl_2-Bn CCT intermediate is lower for electron-withdrawing groups. In the CCT case, the

difference in reorganisation energy is the major factor governing the energy order. Together, these two effects effect an energy difference between the two competing pathways, which is directly linked to the character of the R" group.

Without entropic effects, the energy difference already in the first steps of catalysis by the competing reactions is almost sufficient to explain the selectivity. Were the CCT reactions energetically more favourable by only 12.8 kJ/mol compared to the ATRP reactions, the observed catalytic selectivity based on the R" groups would be fully accounted for. With the approximations employed in the computational study, the agreement is fairly good. Addition of entropic effects suggests that studying only the first step, especially for the CCT pathway, could be insufficient, however. Considering free energies instead of enthalpies increases the energy difference in favour of the ATRP reaction to 51.2 kJ/mol for the R"=PhF complex, which *should* clearly follow the CCT pathway. The main reason for this increase is that the organic ligand attached to iron in the Fe(III)Cl_2-Bn CCT intermediate becomes unbound when entropy is included, indicating an almost immediate decomposition and subsequent reactivity.

The spin-state argument for selectivity still holds, however. The ATRP reactions proceed *via* a high-spin iron complex, and the CCT reaction intermediates are intermediate-spin. Whether the spin state itself is directly important for the catalytic process, or if it simply a consequence of the relative spin state energies, cannot be deduced from the energetic analysis alone. This suggests interesting future research.

On a more general note, this study exemplifies the maturity of quantum chemical modelling of complex reactions involving large transition metal species, also when relative spin-state energies are crucial, and opens up an avenue for further refinement of related catalysts, *in silico*.

ACKNOWLEDGMENTS. We thank Dr. Bertel Westermark and Prof. Miquel Costas for enlightening discussions. The work was performed under the HPC-Europa2 project number 228398 with the support of the European Commission - Capacities Area - Research Infrastructures. It has further been supported by the Ministerio de Ciencia e Innovación (MICINN, project CTQ2008-

06532/BQU), the DIUE of the Generalitat de Catalunya (project 2009SGR528), a MICINN Juan de la Cierva research grant (MPJ), and the Academy of Finland via its Centre of Excellence in Computational Molecular Science, and project 136079. The Barcelona Supercomputing Centre and CSC—The Finnish IT Centre for Science provided abundant parallel computational resources.

REFERENCES

1. M. P. Shaver, L. E. N. Allan, H. S. Rzepa, and V. C. Gibson, *Angew. Chem. Int. Ed.*, 2006, **45**, 1241-1244.
2. M. P. Shaver, L. E. N. Allan, and V. C. Gibson, *Organometallics*, 2007, **26**, 4725-4730.
3. L. E. N. Allan, M. P. Shaver, A. J. P. White, and V. C. Gibson, *Inorg. Chem.*, 2007, **46**, 8963-8970.
4. R. K. O'Reilly, M. P. Shaver, V. C. Gibson, and A. J. P. White, *Macromolecules*, 2007, **40**, 7441-7452.
5. K. Matyjaszewski and J. Xia, *Chem. Rev.*, 2001, **101**, 2921-2990.
6. J.-S. Wang and K. Matyjaszewski, *J. Am. Chem. Soc.*, 1995, **117**, 5614-5615.
7. M. Kato, M. Kamigaito, M. Sawamoto, and T. Higashimura, *Macromolecules*, 1995, **28**, 1721-1723.
8. A. A. Gridnev and S. D. Ittel, *Chem. Rev.*, 2001, **101**, 3611-3660.
9. A. Gridnev, *J. Polym. Sci. A Polym. Chem.*, 2000, **38**, 1753-1766.
10. R. Poli, *Angew. Chem. Int. Ed.*, 2006, **45**, 5058-5070.
11. A. H. Ewald, R. L. Martin, I. G. Ross, and A. H. White, *Proc. R. Soc. London, A*, 1964, **280**, 235-257.
12. P. Gütlich, Y. Garcia, and H. A. Goodwin, *Chem. Soc. Rev.*, 2000, **29**, 419-427.
13. M. A. Halcrow, *Polyhedron*, 2007, **26**, 3523-3576.
14. J. W. Turner and F. A. Schultz, *Coord. Chem. Rev.*, 2001, **219-221**, 81-97.
15. D. R. Hartree, *Proc. Cambridge Phil. Soc.*, 1928, **25**, 89–110.
16. V. Fock, *Z. Phys.*, 1930, **61**, 126–148.
17. C. Møller and M. S. Plesset, *Phys. Rev.*, 1934, **46**, 618–622.
18. J. A. Pople, J. S. Binkley, and R. Seeger, *Int. J. Quantum Chem., Symp.*, 1976, **10**, 1–19.
19. P. Hohenberg and W. Kohn, *Phys. Rev.*, 1964, **136**, B864–B871.
20. W. Kohn and L. J. Sham, *Phys. Rev.*, 1965, **140**, A1133–A1138.
21. M. Swart, M. Solà, and F. M. Bickelhaupt, *J. Chem. Phys.*, 2009, **131**, 094103-9.
22. M. Swart, M. Güell, and M. Solà, *Phys. Chem. Chem. Phys.*, 2011.
23. M. Swart, M. Solà, and F. M. Bickelhaupt, *J. Chem. Theory Comput.*, 2010, **6**, 3145-3152.
24. S. Grimme, *J. Comput. Chem.*, 2006, **27**, 1787–1799.
25. M. Swart, M. Solà, and F. M. Bickelhaupt, *J. Comput. Chem.*, 2011, **32**, 1117-1127.
26. M. P. Johansson and M. Swart, *J. Chem. Theory Comput.*, 2010, **6**, 3302-3311.
27. L. Armangué, M. Solà, and M. Swart, *J. Phys. Chem. A*, 2011, **115**, 1250-1256.
28. A. D. Becke, *Phys. Rev. A*, 1988, **38**, 3098–3100.
29. J. P. Perdew, *Phys. Rev. B*, 1986, **33**, 8822–8824.
30. K. P. Jensen, B. O. Roos, and U. Ryde, *J. Chem. Phys.*, 2007, **126**, 014103-14.
31. G. Brehm, M. Reiher, B. Le Guennic, M. Leibold, S. Schindler, F. W. Heinemann, and S. Schneider, *J. Raman Spectrosc.*, 2006, **37**, 108-122.
32. M. P. Johansson, D. Sundholm, G. Gerfen, and M. Wikström, *J. Am. Chem. Soc.*, 2002, **124**, 11771-11780.
33. M. P. Johansson, M. R. A. Blomberg, D. Sundholm, and M. Wikström, *Biochim. Biophys. Acta*, 2002, **1553**, 183-187.
34. C. Remenyi and M. Kaupp, *J. Am. Chem. Soc.*, 2005, **127**, 11399-11413.
35. C. Rong, S. Lian, D. Yin, B. Shen, A. Zhong, L. Bartolotti, and S. Liu, *J. Chem. Phys.*, 2006, **125**, 174102-7.

36. C. J. Cramer and D. G. Truhlar, *Phys. Chem. Chem. Phys.*, 2009, **11**, 10757-10816.
37. M. Swart, A. R. Groenhof, A. W. Ehlers, and K. Lammertsma, *J. Phys. Chem. A*, 2004, **108**, 5479-5483.
38. M. Swart, *J. Chem. Theory Comput.*, 2008, **4**, 2057-2066.
39. A. Ghosh and P. R. Taylor, *J. Chem. Theory Comput.*, 2005, **1**, 597-600.
40. D. M. A. Smith, M. Dupuis, and T. P. Straatsma, *Mol. Phys.*, 2005, **103**, 273 - 278.
41. F. Weigend and R. Ahlrichs, *Phys. Chem. Chem. Phys.*, 2005, **7**, 3297–3305.
42. K. Eichkorn, O. Treutler, H. Öhm, M. Häser, and R. Ahlrichs, *Chem. Phys. Lett.*, 1995, **240**, 283–290.
43. M. Sierka, A. Hogekamp, and R. Ahlrichs, *J. Chem. Phys.*, 2003, **118**, 9136–9148.
44. F. Weigend, *Phys. Chem. Chem. Phys.*, 2006, **8**, 1057–1065.
45. A. Klamt and G. Schüürmann, *J. Chem. Soc. Perkin Trans. 2*, 1993, 799–805.
46. E. van Lenthe and E. J. Baerends, *J. Comput. Chem.*, 2003, **24**, 1142-1156.
47. P. E. M. Siegbahn, M. R. A. Blomberg, and S.-L. Chen, *J. Chem. Theory Comput.*, 2010, **6**, 2040-2044.
48. J. Ho, A. Klamt, and M. L. Coote, *J. Phys. Chem. A*, 2010, **114**, 13442-13444.
49. J. Neugebauer and B. A. Hess, *J. Chem. Phys.*, 2003, **118**, 7215-7225.
50. R. Ahlrichs, M. Bär, M. Häser, H. Horn, and C. Kölmel, *Chem. Phys. Lett.*, 1989, **162**, 165–169.
51. M. von Arnim and R. Ahlrichs, *J. Comput. Chem.*, 1998, **19**, 1746–1757.
52. G. te Velde, F. M. Bickelhaupt, E. J. Baerends, C. F. Guerra, S. J. A. van Gisbergen, J. G. Snijders, and T. Ziegler, *J. Comput. Chem.*, 2001, **22**, 931-967.
53. C. Fonseca Guerra, J. G. Snijders, G. te Velde, and E. J. Baerends, *Theor. Chem. Acc.*, 1998, **99**, 391-403.
54. K. Eichkorn, F. Weigend, O. Treutler, and R. Ahlrichs, *Theor. Chem. Acc.*, 1997, **97**, 119–124.
55. M. P. Johansson and D. Sundholm, *J. Chem. Phys.*, 2004, **120**, 3229–3236.
56. I. García-Rubio and G. Mitrikas, *J. Biol. Inorg. Chem.*, 2010, **15**, 929-941.
57. E. A. Mader, E. R. Davidson, and J. M. Mayer, *J. Am. Chem. Soc.*, 2007, **129**, 5153-5166.
58. F. L. Hirshfeld, *Theoret. Chim. Acta*, 1977, **44**, 129-138.
59. R. A. Marcus and N. Sutin, *Biochim. Biophys. Acta*, 1985, **811**, 265-322.
60. E. I. Davydova, T. N. Sevastianova, A. Y. Timoshkin, A. V. Suvorov, and G. Frenking, *Int. J. Quantum Chem.*, 2004, **100**, 419-425.
61. M. P. Johansson and M. Patzschke, *Chem. Eur. J.*, 2009, **15**, 13210-13218.
62. J. P. Perdew and Y. Wang, *Phys. Rev. B*, 1986, **33**, 8800–8802.
63. W. Kutzelnigg and J. D. Morgan, *Z. Phys. D*, 1996, **36**, 197-214.
64. A. D. Becke, *J. Chem. Phys.*, 1993, **98**, 5648–5652.
65. C. Lee, W. Yang, and R. G. Parr, *Phys. Rev. B*, 1988, **37**, 785–789.
66. M. Reiher, O. Salomon, and B. A. Hess, *Theor. Chem. Acc.*, 2001, **107**, 48-55.
67. M. Radoń and K. Pierloot, *J. Phys. Chem. A*, 2008, **112**, 11824-11832.